

Intracavity Brillouin gain characterization based on cavity ringdown spectroscopy

ANANTHU SEBASTIAN¹, STÉPHANE TREBAOL^{1,*}, AND PASCAL BESNARD¹

¹Univ Rennes, CNRS, Institut FOTON - UMR 6082, F-22305 Lannion, France

*Corresponding author: stephane.trebaol@enssat.fr

Compiled November 1, 2021

We report a technique based upon the cavity ringdown method that enables to characterize the Brillouin gain coefficient directly in a laser cavity. Material gain, optical cavity parameters and lasing properties can be extracted from measurements within a single experiment. © 2021 Optical Society of America

<http://dx.doi.org/10.1364/ao.XX.XXXXXX>

1. INTRODUCTION

The constant need for laser spectral purity improvements is driven by the growing panel of applications in fundamental [1, 2] and applied physics [3, 4]. One of the most promising approach to generate compact and narrow linewidth lasers is based on the stimulated Brillouin scattering (SBS) optical nonlinearity [5]. The establishment of SBS in an optical cavity [6] gives rise to the coherent emission of a Stokes wave. Impressive noise performances have been reported in such Brillouin lasers [7–9]. To reach such high laser performances, one of the most important parameters to evaluate is the material gain coefficient. The Brillouin gain coefficient, can be expressed in function as material parameters by [10]:

$$g_B = \frac{2\pi n^7 p_{12}^2}{c\rho_0 \lambda_p^2 \Delta\nu_B V_A} \quad (1)$$

where c is the vacuum velocity of light, λ_p the laser pump wavelength and $\Delta\nu_B$ is the Full Width at Half Maximum (FWHM) of the Brillouin gain. Other parameter values are given in table 2. Usually, the g_B may be estimated through classical pump-probe experiments [11], self-heterodyne [12], Fabry-Perot interferometry [5] or threshold power determination [13, 14]. In those methods, the SBS phenomenon is generated by injecting a pump power signal in a single-pass waveguide. Close to SBS threshold, a Stokes signal can be efficiently created in the counter propagating direction of the incident pump. The Stokes frequency is downshifted from the pump frequency by the Stokes shift ν_B . The associated gain profile is described by:

$$g_B(\nu) = g_B \frac{(\Delta\nu_B/2)^2}{(\nu - \nu_B)^2 + (\Delta\nu_B/2)^2} \quad (2)$$

Probing the gain profile by above mentioned methods allows to determine $\Delta\nu_B$. Then introducing $\Delta\nu_B$ value and material

constants, extracted by other experimental means or from calculations, into Eq. (1) gives a Brillouin gain coefficient estimation. Those methods suffer from several drawbacks. First, to reach the SBS threshold, one have to either use long waveguide [13] or high pump power [14], which are not always suitable depending on the material and cavity design (waveguide, microresonator). And secondly, the g_B parameter can be inferred at the expense of knowing material constants, which are not systematically available depending on the material under study.

The cavity ringdown method (CRDM) has been successfully implemented in various optical cavities [15–17] to determine coupling regime and dispersive properties [15], selective amplification in erbium doped media [18], mode coupling [19] and nonlinear parameters [20, 21].

In this letter, we propose to extend the use of the CRDM to retrieve the Brillouin gain coefficient. Performing Brillouin gain characterization inside the laser cavity allows to take advantage of the light recirculation of the Stokes wave inside the resonator. In fact, this tends to strongly reduce the length of the waveguide and the applied laser-pump power required to reach the SBS threshold in comparison to usual pump-probe techniques. Moreover, the gain coefficient is retrieved without the need of material parameter values. It allows also to identify several nonlinear processes that can occur for example in high-Q resonator as thermal drift and Kerr effect [21].

The paper is organized as follows : First, we describe the procedure to retrieve the intracavity Brillouin gain coefficient from the CRDM technique. Then, we detail the experimental bench used to generate and probe the SBS gain in the cavity and finally we detail and discuss our results.

2. PRINCIPLE

Figure 1 b) recalls the spectral arrangement of waves taking part in the SBS process when studied in a resonant cavity. The blue line corresponds to the pump signal at frequency ν_p that produces a Stokes gain (green curve, Eq. (2)) through the SBS process. In the background of the figure, the periodic distribution of the ring cavity modes are colored in gray. In our configuration, the pump signal is not resonant within a cavity round-trip. Nevertheless, the perimeter of the resonator, that fixed the free spectral range of the cavity ($\Delta\nu_{FSR}$), and the spectral gain distribution insure to favor the amplification of one cavity mode (red color line), that we call the Stokes-mode. We consider that the Stokes-mode at the frequency ν_S is seeded at

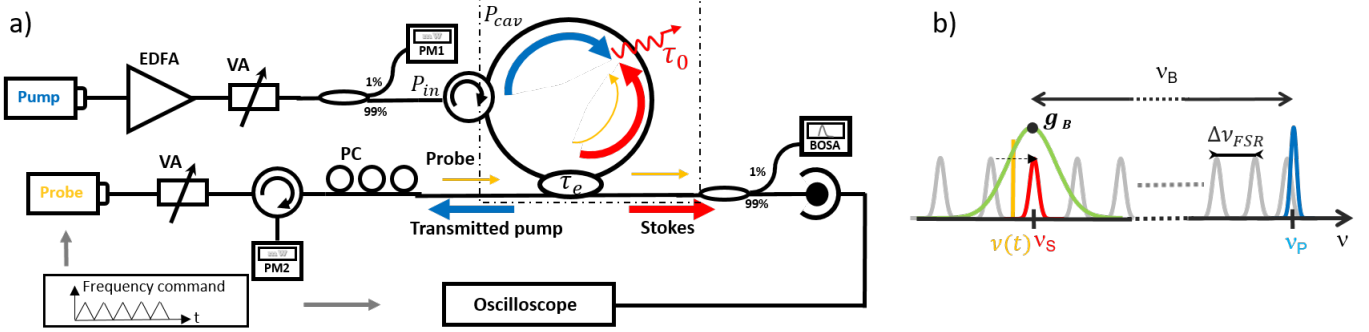


Fig. 1. a) Experimental setup for Brillouin gain cavity ringdown determination. EDFA: Erbium-doped fiber amplifier, VA: variable attenuator, PC: polarization controller, BOSA: Brillouin optical spectrum analyzer, PM : Powermeter. b) Spectral overview of the CRDM method. Pump laser line (blue), Brillouin gain curve (green), probed cavity mode (red) and probing laser line (yellow). v_B corresponds to the Brillouin shift, where Δv_{FSR} stands for the spectral spacing between cavity modes.

the maximum of the gain value g_B .

We have now to determine how the Stokes-mode linear-losses might be compensated by the Brillouin gain as a function of the incident pump power P_{in} . The following model description is based on the coupled mode theory described elsewhere [15, 22] and adapted to the present study for the purpose of Brillouin gain characterization.

The resonator schematic is shown in Fig. 1 a) (dashed square). We consider the temporal amplitude evolution $u_S(t)$ of the Stokes-mode. Its total photon lifetime $\tau/2$ experienced by this cavity mode is:

$$\frac{1}{\tau} = \frac{1}{\tau_0} + \frac{1}{\tau_e} \quad (3)$$

where $\tau_0/2$ and $\tau_e/2$ are the intrinsic photon and the coupler lifetimes respectively. The intrinsic photon lifetime expresses the losses or gain of the cavity while the coupler lifetime relates to the coupling strength between the cavity and the input/output fiber. We can relate the coupling coefficient $|\kappa|^2$ and the intensity round-trip attenuation a^2 to their respective photon lifetime. Indeed, in the high finesse approximation ($|\kappa|^2 \times a^2 \approx 1$) [23], the coupler lifetime can be related to the coupling coefficient by $|\kappa|^2 = 2\tau_L/\tau_e$ where τ_L is the photon round-trip time. The intrinsic photon lifetime τ_0 is related to the intensity round trip attenuation a^2 by:

$$a^2 = 1 - 2\tau_L/\tau_0 \quad (4)$$

Then a positive τ_0 corresponds to an optical attenuation with $a^2 < 1$ while a negative τ_0 implies optical Brillouin gain with $a^2 > 1$. Moreover, the intensity round-trip attenuation of the Stokes-mode can be expressed as:

$$a^2 = \beta \times e^{-\alpha_L L} e^{g_B P_{cav} L_{eff}/A_{eff}} = a_{op}^2 e^{g_B P_{cav} L_{eff}/A_{eff}} \quad (5)$$

where β is the inner local losses including the contribution of splices, circulator and coupler; α_L the fiber-loss coefficient; A_{eff} the effective fiber-mode area. L and L_{eff} are respectively the cavity length and the effective interaction length. a_{op}^2 is the intensity round-trip attenuation of the cold cavity mode without stimulated Brillouin scattering. Here P_{cav} is the nonresonant intracavity pump power.

As can be seen in Eq. (5), increasing the pump intensity P_{cav} , allows the resonator linear losses experienced by the Stokes-mode to be compensated over a single round-trip. Thereby, intensity round-trip attenuation a^2 and intrinsic photon lifetime

τ_0 can be tuned through pump intensity keeping constant the coupler lifetime.

τ_0 can be evaluated experimentally using the CRDM technique and therefore a_0^2 and a^2 . Indeed, the probe signal coupled in the Stokes mode, through the coupler, will experience attenuation or amplification within a round-trip. It follows that, experimental estimation of the Brillouin gain coefficient can be obtained by using Eq. (4) together with Eq. (5):

$$g_B = \frac{A_{eff}}{P_{cav} L_{eff}} \ln \frac{a^2}{a_{op}^2} \quad (6)$$

The CRDM technique consists in probing the Stokes-mode by sweeping the frequency of a tunable narrow linewidth laser (yellow color line on Fig. 1) across the resonance. The sweeping speed of the laser is tuned sufficiently fast to observed ringing phenomenon characteristic from the transient response of the cavity. In its current version, our experimental bench allows to study resonator Q-factor as low as 10^7 . The ringing effect is a signature of interferences between the probing laser and the cavity mode waves at the output of the coupler. In a previous paper [15], we have determined an analytical expression for the transient response of a resonator as function of τ_0 , τ_e and the sweeping speed. By use of a least square method, this expression can be used to retrieve the resonator lifetimes and then the Brillouin gain coefficient as shown on Fig. 2.

3. EXPERIMENTAL SETUP

The experimental setup is presented in Fig. 1 a). The fiber cavity is composed of a $L = 20$ m polarization maintaining silica fiber distributed as $L_1 = 19$ m from coupler to isolator and $L_2 = 1$ m between isolator and coupler. Fiber length uncertainty is of the order of ± 0.6 m. This cavity length giving a free spectral range (FSR) of $\Delta v_{FSR} = 10 \pm 0.3$ MHz. The transient response acquired by the CRDM technique results from the beating between the transmitted probe and the output coupled Stokes-mode at the output of the coupler. The intensity of the probe, seeded in the Stokes-mode, has to be precisely determined after one round-trip. It is related to the input probe at the coupler position by the intensity round-trip attenuation (see Eq. (5)). The effective interaction length have to be precisely determined to optimized the evaluation of g_B . For our cavity configuration, $L_{eff} = L_1 + |t^2| \times L_2 = 19.9 \pm 0.6$ m where the coupler transmission coefficient $|t^2| = (1 - |\kappa|^2)$ is introduced to incorporate the

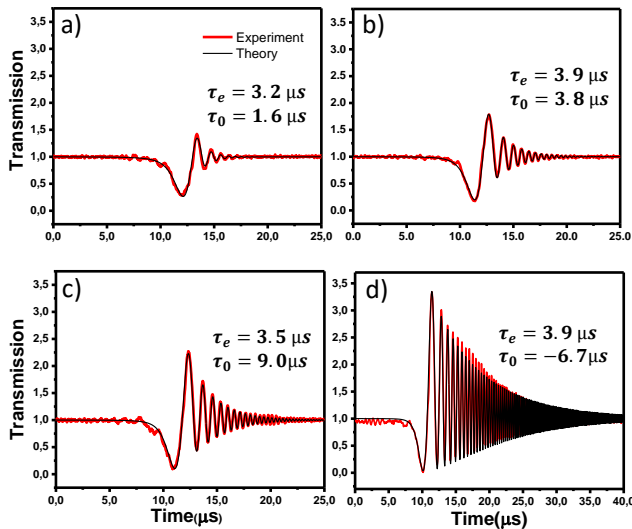


Fig. 2. Transient responses of the probed cavity mode for various laser pump powers. From a) to d) the resonator-coupling regime shifts with increasing pump power from under coupling ($P_{in} = 13.8$ mW), critical coupling ($P_{in} = 39.1$ mW), over coupling ($P_{in} = 41.7$ mW) and selective amplification regime ($P_{in} = 58.5$ mW).

pump intensity attenuation through the coupler. The effective area of the fiber is $A_{eff} = 84.9 \pm 0.2 \mu\text{m}^2$. A part of the Stokes wave is extracted from the resonator through a 95/5 coupler. Let's first describe the SBS setup. The laser pump intensity of a single mode laser with 250 kHz linewidth centered at 1550 nm, is first amplified through an EDFA and then adjusted by a variable attenuator. 1 % of the pump is extracted through a coupler for intensity power monitoring (PM1). The nonresonant intracavity pump power P_{cav} is determined just after the circulator and can be related to P_{in} by $P_{cav} = \alpha \times P_{in}$ where $\alpha = 0.758$ is the relative losses experimentally evaluated. The circulator ensures a single pass of the pump signal within the fiber loop preventing re-injection. For sufficiently intense pump intensity, stimulated Brillouin Stokes signal is generated in the opposite direction of the pump signal. Extracted Stokes signal is analyzed spectrally through a high resolution BOSA and the intensity is recorded by a photodiode. The lasing threshold is determined when pump depletion starts corresponding to a pump power P_{th} equal to 62 mW.

We will now describe the CRDM setup. All the measurements are performed for a pump power P_{in} lower than the pump power lasing threshold P_{th} (corresponding to a range of 1-100 mW in our main set-up) to be within the valid domain of the technique [15]. The probe signal is provided from a tunable laser with 250 kHz linewidth. Before entering the cavity, the signal intensity is controlled by a variable attenuator (VA) and its polarization adjusted through polarization controller (PC). The probe laser frequency is positioned close to the Stokes-mode with the help of the 10 MHz-resolution BOSA. The probe frequency is continuously swept across the resonant Stokes signal by a frequency command allowing the sweeping speed and the scanned frequency range to be adjusted. The transmission of the cavity mode is then collected by a photodiode and observed on an oscilloscope triggered by the frequency command.

4. RESULTS

CRDM signals are collected for input pump powers varying from 0 to P_{th} . Figure 2 presents various CRDM signals collected for pump power ranging from 13.8 to 58.5 mW (red color curves). The normalized transmission is plotted as function of time. For increasing pump power, the amplitude, the number and the frequency of oscillations increase. To get more insight on those specific temporal signatures, data are fitted using the procedure described above and allows to determine τ_0 and τ_e as function of P_{in} (See Fig. 2). As expected the τ_e value is constant over all the measurements because the coupler losses are fixed. For $P_{in} = 0$ mW, the cold cavity parameters are extracted and gives $\tau_e = 3.8 \mu\text{s}$ and $\tau_0 = 1.2 \mu\text{s}$. Using the definition $Q = 2\pi\nu_S\tau/2$ gives an estimated quality factor of 5.6×10^8 . For $P_{in} = 13.8$ to 50.1 mW, τ_0 increases, modifying the coupling regime from under-coupling (cold cavity) to the critical coupling, the overcoupling and finally the transparency regime. For $50.1 \text{ mW} < P_{in} < P_{th}$, τ_0 takes a negative value corresponding to the amplification regime. Indeed, the variation of τ_0 as function of the pump power refers to a progressive compensation of the linear losses until the amplification regime.

From those fitted datas, we are able to retrieve a^2 (Eq. (5)) and

Table 1. Comparison of g_B values obtained for single mode silica fiber [24] in various works. SH stands for Self-Heterodyne.

Methods	g_B value	standard deviation
	$[\times 10^{-11} \text{ m/W}]$	$[\pm 10^{-12} \text{ m/W}]$
CRDM [our work]	1.94	1.5
SH [silica value]	2.45	1.8
SH [3% GeO_2 value]	1.92	1.4
Pump-probe [25]	2.29	-

Table 2. Material values for pure and 3% GeO_2 doped silica fibers.

Parameters	SiO_2	$\text{SiO}_2 + 3\% \text{GeO}_2$
	[25]	[26]
Refractive index [n]	1.45	1.46
Elasto-optic coefficient [p_{12}]	0.271	0.236
Density [$\rho(\text{kg.m}^{-3})$]	2200	2244

then the value of the Brillouin gain g_B by use of Eq. (6). This procedure is applied for each pump power giving estimations of the Brillouin gain parameter. Figure 3 summarized the extracted gain values as function of the pump power. The mean value (red dashed line) is equal to $1.94 \times 10^{-11} \text{ m/W}$ with a standard deviation (shaded green region) of $\pm 1.5 \cdot 10^{-12} \text{ m/W}$. The uncertainty contribution to g_B related to A_{eff} , L_B and P_{cav} gives $0.6 \times 10^{-12} \text{ m/W}$ and do not enlarge the experimentally determined standard deviation of g_B . We can then conclude that the Brillouin gain standard deviation is related to the experimental extraction of τ_0 .

To evaluate the pertinence of the method, we compare our

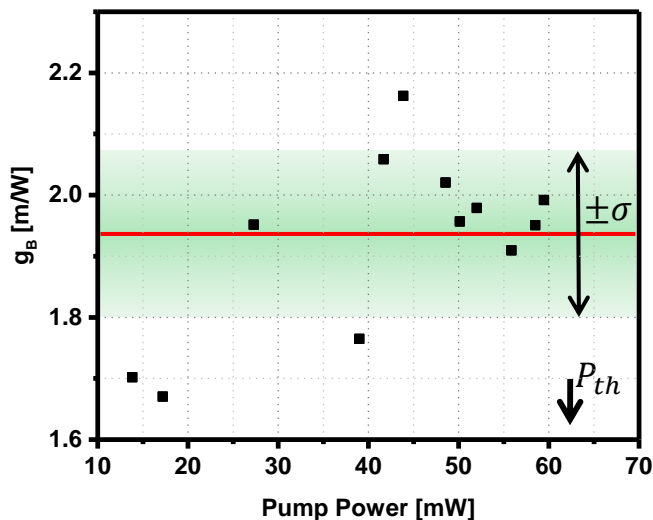


Fig. 3. Brillouin gain coefficient extracted from the CRDM signal for various input pump power. The mean value is equal to $g_B = 1.94 \times 10^{-11} \pm 1.5 \times 10^{-12} \text{ m/W}$. This measure of g_B value is compared to other works in Tab. 1

CRDM technique to usual self-heterodyne method [12]. The Brillouin gain bandwidth is experimentally estimated to $\Delta\nu_B = 27.5 \pm 2$ MHz. Then, using Eq. (1), gain coefficient can be determined. As mentioned before, this determination depends on material parameters of the used fiber. Fabrication process conditions (doping, temperature, etc.) affect those parameters. For example, a commercial single mode fiber in the C band region has usually a GeO_2 -doping concentration of few percents but this value is usually unknown precisely. We report in table 2 material values for pure silica and 3%-doped GeO_2 silica fiber. Using those parameters, Brillouin gain estimation gives 2.45 and $1.92 \times 10^{-11} \text{ m/W}$ (see Table 1) respectively. The standard deviation, related to $\Delta\nu_B$ determination, is bounded between $\pm 1.4 \times 10^{-12} \text{ m/W} < \sigma < 1.8 \times 10^{-12} \text{ m/W}$. Our g_B determination is very close from the one obtained by self-heterodyne using the parameters of a commercial monomode fiber 3%-doped with GeO_2 . Upon this example, we see that the material parameters strongly impact the estimation of the Brillouin gain. Comparison to other works on similar silica fibers (see Tab. 1) give comparable g_B values.

5. CONCLUSION

A cavity ringdown method is applied to stimulated Brillouin scattering in fiber cavity. Contrary to usual techniques, this new method gives access, through a simple and single measurement, as well to the Brillouin gain coefficient of the fiber material as to the cavity parameters. We have shown that the fast sweeping ringdown technique allows Brillouin gain to be characterized. The proof of concept has been experimentally demonstrated with a silica fiber ring resonator. This allowed us to determine unambiguously the coupling regime and to estimate the Brillouin gain coefficient of the material composing the resonator without the needs of material constants knowledge. The comparison to usual pump-probe techniques gives good agreements. This cavity ringdown method can be applied to any kind of resonators allowing for example, the determination of Brillouin

gain coefficient in microresonators, exotic material fiber rings and whispering gallery mode resonators.

The present work is supported under project FUI AAP20 SOLBO, with the help of BPI FRANCE and Pôle Images & Réseaux. We thank also UBL for its financial support.

The authors would like to thank P. Féron and Y. Dumeige for fruitful discussions and for their careful reading of the manuscript.

REFERENCES

1. Y. Jiang, A. Ludlow, N. D. Lemke, R. W. Fox, J. A. Sherman, L.-S. Ma, and C. W. Oates, *Nat. Photonics* **5**, 158 (2011).
2. K. Predehl, G. Grosche, S. Raupach, S. Droste, O. Terra, J. Alnis, T. Legero, T. Hänsch, T. Udem, R. Holzwarth *et al.*, *Science* **336**, 441 (2012).
3. J. Geng, C. Spiegelberg, and S. Jiang, *IEEE Photonics Technol. Lett.* **17**, 1827 (2005).
4. P. J. Rodrigo and C. Pedersen, *Opt. Express* **18**, 5320 (2010).
5. E. Ippen and R. Stolen, *Appl. Phys. Lett.* **21**, 539 (1972).
6. S. Smith, F. Zarinetchi, and S. Ezekiel, *Opt. letters* **16**, 393 (1991).
7. W. Loh, J. Becker, D. C. Cole, A. Coillet, F. N. Baynes, S. B. Papp, and S. A. Diddams, *New J. Phys.* **18**, 045001 (2016).
8. M.-G. Suh, Q.-F. Yang, and K. J. Vahala, *Phys. review letters* **119**, 143901 (2017).
9. A. Sebastian, I. V. Balakireva, S. Fresnel, S. Trebaol, and P. Besnard, *Opt. Express* **26**, 33700 (2018).
10. G. P. Agrawal, "Nonlinear fiber optics," in *Nonlinear Science at the Dawn of the 21st Century*, (Springer, 2000), pp. 195–211.
11. N. Shibata, R. G. Waarts, and R. P. Braun, *Opt. letters* **12**, 269 (1987).
12. R. Tkach, A. Chraplyvy, and R. Derosier, *Electron. Lett.* **22**, 1011 (1986).
13. D. Cotter, *Electron. Lett.* **18**, 495 (1982).
14. K. S. Abedin, *Opt. Express* **13**, 10266 (2005).
15. Y. Dumeige, S. Trebaol, L. Ghiša, T. K. N. Nguyen, H. Tavernier, and P. Féron, *JOSA B* **25**, 2073 (2008).
16. G. N. Conti, S. Berneschi, F. Cosi, S. Pelli, S. Soria, G. C. Righini, M. Dispenza, and A. Secchi, *Opt. Express* **19**, 3651 (2011).
17. R. Henriët, G. Lin, A. Coillet, M. Jacquot, L. Furfaro, L. Larger, and Y. K. Chembo, *Opt. letters* **40**, 1567 (2015).
18. A. Rasoloniaina, V. Huet, T. K. N. Nguyen, E. Le Cren, M. Mortier, L. Michely, Y. Dumeige, and P. Féron, *Sci. Reports* **4**, 4023 (2014).
19. S. Trebaol, Y. Dumeige, and P. Féron, *Phys. Rev. A* **81**, 43828 (2010).
20. A. A. Savchenkov, A. B. Matsko, M. Mohageg, and L. Maleki, *Opt. Lett.* **32**, 497 (2007).
21. A. Rasoloniaina, V. Huet, M. Thual, S. Balac, P. Féron, and Y. Dumeige, *JOSA B* **32**, 370 (2015).
22. H. A. Haus, *Waves and fields in optoelectronics* (Prentice-Hall, 1984).
23. A. Yariv, *Electron. Lett.* **36**, 321 (2000).
24. "Corning smf-28 ultra optical fiber," <https://www.corning.com/media/worldwide/coc/documents/Fiber/SMF-28%20Ultra.pdf>, note = Accessed 24 May 2019.
25. P. D. Dragic, *J. Light. Technol.* **29**, 967 (2011).
26. N. Lagakos, J. A. Bucaro, and R. Hughes, *Appl. Opt.* **19**, 3668 (1980).